

**RESEARCH ARTICLE**

10.1002/2017JB015190

**Special Section:**

Magnetism in the Geosciences  
- Advances and Perspectives

**Key Points:**

- Fine grained nanometer-sized magnetite, maghemite, and hematite are the main iron oxides in burnt daub remains from Neolithic houses
- Paleo-firing temperatures determined with magnetic susceptibility method are notably high; they range between 680 and 1,140°C
- Iron oxides' magnetic properties resemble those of particles synthesized by the solution combustion method

**Supporting Information:**

- Supporting Information S1
- Data Set S1

**Correspondence to:**

N. Jordanova,  
neli\_jordanova@hotmail.com

**Citation:**

Jordanova, N., Jordanova, D., Kostadinova-Avramova, M., Lesigysarski, D., Nikolov, V., Katsarov, G., & Bacvarov, K. (2018). A mineral magnetic approach to determine paleo-firing temperatures in the Neolithic settlement site of Mursalevo-Deveboaz (SW Bulgaria). *Journal of Geophysical Research: Solid Earth*, 123. <https://doi.org/10.1002/2017JB015190>

Received 1 NOV 2017

Accepted 16 MAR 2018

Accepted article online 24 MAR 2018

## A Mineral Magnetic Approach to Determine Paleo-Firing Temperatures in the Neolithic Settlement Site of Mursalevo-Deveboaz (SW Bulgaria)

Neli Jordanova<sup>1</sup> , Diana Jordanova<sup>1</sup>, Maria Kostadinova-Avramova<sup>1</sup>, Deyan Lesigysarski<sup>1</sup>, Vassil Nikolov<sup>2</sup>, Georgi Katsarov<sup>3</sup>, and Krum Bacvarov<sup>2</sup>

<sup>1</sup>National Institute of Geophysics, Geodesy and Geography, Bulgarian Academy of Sciences, Sofia, Bulgaria, <sup>2</sup>National Institute of Archaeology and Museum, Bulgarian Academy of Sciences, Sofia, Bulgaria, <sup>3</sup>Freelance Archaeologist

**Abstract** Archeological remains from the Neolithic period in SE Europe are characterized by the presence of massive burnt daub relics sintered at high temperatures. These findings raised the hypothesis of deliberate house burning as a strategy for ensuring the survival of place and the development of social memory in Neolithic society. Although highly discussed in the archeological community, analytical data on the ancient firing temperatures achieved during burning Neolithic houses are missing except an empirical study determining firing temperatures according to the color of burned clay. The Neolithic site Mursalevo-Deveboaz (Bulgaria) is one of the largest known settlements consisting of more than 70 houses. Rock-magnetic analyses are applied for characterization of iron oxides produced during firing, and the firing temperatures were estimated using the magnetic susceptibility method. Results on a collection of 445 samples show the presence of very fine grained magnetite/maghemite and hematite. Magnetic data are supported by elemental analysis, reflectance spectroscopy, and scanning electron microscopy. The data suggest an increase in the magnetic grain size from superparamagnetic toward single domain with increasing firing temperature. Firing temperature estimates for 148 samples of different color vary between 680 and 1,140°C. Comparing the magnetic properties of iron oxides identified and literature data on solution-combustion synthesis of iron oxides allowed a mechanism behind the extreme firing of Neolithic houses to be suggested. Our study proposes for the first time that combustion synthesis of iron oxides could explain the extreme house burning in many Neolithic settlements achieved through intentional addition of wood, dung and urine.

### 1. Introduction

Paleo-firing temperatures are important indicators for reconstructions of characteristics of lava flows and their influence on the host rocks (e.g., Mare et al., 2016; Silva et al., 2006), as well as for constraining the maximum temperature achieved in the rupture zone during an earthquake (e.g., Yang et al., 2016). Furthermore, determination of (paleo)firing temperatures is of great importance in archeology and specifically for pottery characterization in order to ascertain the technological development and/or provenance of the finds (Maniatis, 2009) or to document the human use of fire in sediments (Barbetti, 1986; Carrancho et al., 2016; Kapper et al., 2014). Different analytical methods are employed for such analysis (mineralogical studies, scanning electron microscopy (SEM), color determination, Mössbauer spectroscopy, thermal analysis, etc.) which are based on examination of the progressive change in physical properties of burnt clay upon increased temperature (Murad & Wagner, 1998). Mineral magnetism provides another sensitive tool for estimation of (paleo)firing temperatures because of the well-established fundamentals of magnetism of iron oxides during thermal transformations (Dunlop & Özdemir, 1997).

Apart from pottery, sintered daub remains provide important information about the firing conditions and the interpretation of structural burning in the archeological record (Harrison, 2013). Daub is defined as a mixture of clay and various organic fibrous materials (e.g., straw, grass, and animal dung) used for house construction in ancient times (Kruger, 2015). Magnetic and mineral magnetic studies on daub materials are limited and related to archaeomagnetic dating of these remains (Guerrero et al., 2016; Shaffer, 1993; Salisbury et al., 2013). The phenomenon of burnt houses in the later prehistory (sixth and fifth millennia B.C.) of Southeast Europe is a well-known fact evidenced at numerous archeological sites across the Balkans (Brami, 2014; Chapman, 1999; Stevanović, 1997; Tringham, 2013) and Anatolia (Akkermans et al., 2012; Love, 2013;

Verhoeven, 2000). Several hypotheses about the reasons of these extensive fires have been suggested. As Chapmann (1999) emphasized in his review, the hypotheses of an accidental origin of the fires or local criminal wars cannot fully explain the archeological finds in their entity. Nowadays archeologists often accept the theory of deliberate burning of houses, even though the reasons for this remain a matter of speculation. A major indirect argument in favor of the deliberate burning theory is that no modern experiment on simulating accidental fire in wattle-and-daub houses succeeded to achieve the degree of burning found at Neolithic burnt houses (Chapmann, 1999; Gheorghiu, 2009).

Focused research on estimations of the firing temperatures achieved during the burning of houses at Neolithic settlement sites in Southeast Europe is limited to the empirical determinations based on color evaluation, done by Stevanović (1997) for the Vinča culture site of Opovo in Serbia. The author reports major firing temperatures in the interval 500–800°C, and only a very limited number of rubble displaying signs of the strong sintering and vitrification suggest temperatures in the interval 900–1,200°C. Other research on the mechanisms and reasons of house burning at Neolithic sites in Southeast Europe was mostly focused on ethno-archeological considerations (Brami, 2014; Chapmann, 1999; Kruger, 2015).

Thus, the main aim of this study is to employ mineral magnetic investigations in order to provide an analytical evaluation of the firing temperatures of the burnt daub material collected from the Neolithic site of Mursalevo-Deveboaz. Furthermore, the application of rock-magnetic techniques yields additional information about the iron oxide products of firing and gives possible clues on the mechanism of firing. The Neolithic settlement site of Mursalevo-Deveboaz in the Middle Struma Valley (southwest Bulgaria) was recently uncovered during rescue excavations. Taking into account the archeological findings which suggest that almost all houses throughout the site's occupation were destroyed by fires, one of our main objectives here is to test the deliberate house burning theory by checking the archeological evidence against the results of the rock-magnetic analyses.

## 2. The Archeological Site of Mursalevo-Deveboaz

The site of Mursalevo-Deveboaz was first discovered during the construction of a railroad in the late 1920s (Mikov, 1932) but was excavated only recently in 2014–2015 (Nikolov et al., 2015a, 2015b, 2016), during the construction of the Struma Highway. The site covers a total area of over 5 acres on the left bank of the Struma River, in a narrower part of the river's middle valley south of the modern village of Mursalevo, southwest Bulgaria (Figure 1a).

An area of about 2.5 acres was completely excavated (Figure S1 in the supporting information) accounting for roughly one-third of a prehistoric village dating to a later phase of the local Early Neolithic (EN) (ca. 5700–5500 B.C.). A radiocarbon dating project is in progress, but no dates are yet available. Thus, relative dating of the site is based on assessment of material culture assemblages. In the Late Neolithic (LN) (~5400–4900 B.C.), the village relocated immediately north and east of the EN settlement area, with a partial overlapping of EN and LN layers only in an additionally exposed long and narrow area in the easternmost part of the site. Also, remains from later occupations in the Late Iron Age (late first mill. B.C.) and the early Middle Ages (seventh and eighth century A.D.) were identified.

The results of the magnetic survey in advance of the excavation showed a well-organized orthogonal plan of the latest occupation phases of the EN village, with the houses built along a grid of alleys, between two ravines to the north and south, and the river bed to the west. The excavations revealed that more or less the same pattern had been followed since the earliest occupation phases. The remains of 62 EN and 13 LN houses were unearthed (Figures S1 and S2), most of them being two-story, with the ground floor area measuring between 30 and 100 m<sup>2</sup>. They were built of a wood-and-daub construction. The wattle-and-daub technique that was common for the southeast European later prehistory has only sporadically been used. The walls were made of densely fixed posts, and the floor of the second story was made of boards plastered with a thick layer of daub. Most of the investigated EN houses (52 or 83.87%) and all of the LN ones were destroyed by fire, and the archeological evidence seems to suggest that the fires were the results of deliberate acts. The major arguments in favor of this theory are summarized in the supporting information. Admittedly, all of this archeological evidence is circumstantial and therefore needs verification by scientific techniques such as the application of rock-magnetic methods.



**Figure 1.** (a) The Neolithic site of Mursalevo-Deveboaz. Aerial photograph of the site after the removal of the topsoil. In the inset, (right) Balkan Peninsula with study area outlined; (left) Struma river valley with site location; (b) burned daub and vitrified material from house 24.

### 3. Sampling and Methods

#### 3.1. Sampling

During the 2014 excavation season, 445 nonoriented samples from daub remains were taken from different parts of the site, including EN and LN houses. Daub samples were collected from 25 Neolithic houses uncovered at that stage of the archeological excavation. Differently colored daub pieces were sampled from each investigated structure, rough sketches of the position of the respective samples in the houses, and, where possible, their origin according to the excavators (wall, floor of the second story, grain storage bin, pottery, etc.) were logged in the field book. Burned areas exhibited diverse coloring varying from black-purple-brown to red-orange-yellow (Figure 1b).

It was anticipated that the raw material for house construction at Mursalevo-Deveboaz comes most probably from the surrounding outcropping sediments. Therefore, sediment deposits were sampled from an exposed profile (the wall of an excavated Neolithic pit, no. 173, square K29, dug in anthropogenically unaffected sediment). Loose sediment samples from 7 depth intervals down to 125-cm depth were collected. This sampling scheme aimed at probing sediment material representative of different layers which might have been used for house construction by the Neolithic people. In the laboratory, samples were left to air dry and were further used for magnetic and nonmagnetic measurements. Cubic ( $2 \times 2 \times 2$  cm) samples from 148 daub pieces from different houses were cut for employing the refring/magnetic susceptibility method (Rasmussen et al., 2012) for determination of the ancient firing temperature. The method relies on the magnetic susceptibility changes of fired clay upon laboratory incremental heating, assuming that the most significant changes reflect crossing the threshold temperature of the ancient firing. The color of the daub samples was determined with the Munsell Soil Color chart (data set provided in the supporting information).

#### 3.2. Laboratory Magnetic Measurements

Magnetic susceptibility was measured with an MFK-1A magnetic susceptibility bridge (AGICO Ltd., Czech Republic) with a sensitivity  $1 \times 10^{-8}$  SI, operating frequency 976 Hz, and field strength of 200 A/m. Frequency-dependent magnetic susceptibility ( $\chi_{fd}$ ) was measured with a Bartington MS2 kappa meter with MS2B dual frequency sensor (0.465 kHz low frequency [LF]) or 4.65 kHz (high frequency [HF]) (Bartington Instruments Ltd., UK) with maximum resolution  $2 \times 10^{-6}$  SI. The relative abundance of the superparamagnetic (SP) fraction in the bulk magnetic assemblage is evaluated through the parameter  $\chi_{fd}\%$  defined as  $\chi_{fd}\% = 100 * (\chi_{LF} - \chi_{HF})/\chi_{LF}$ . Frequency-dependent magnetic susceptibility defined as  $\chi_{fd} = \chi_{LF} - \chi_{HF}$  is also used as an indication about the absolute contribution of the fine SP grains in the total magnetic assembly. Magnetic susceptibility was expressed on a mass-specific basis by dividing the measured values by the sample's mass and accounting for actual volume. Stepwise incremental heating was performed in a shielded furnace MMTD20 (Magnetic Measurements Ltd., UK) up to 800°C and in a Nabertherm Laboratory Muffle furnace L 3/12 (Nabertherm GmbH, Germany) with maximum nominal temperature 1,200°C up to 1,000 or 1,180°C. Heating step of 50°C was applied from 300 to 550°C and steps of 20°C from 550 to 1180°C. At the first heating temperature (300°C), all the samples were heated for 1.5 hr, and after that, samples were kept at the respective temperature for 1 hr. For temperatures above 900°C, this time was reduced to 40 min.

The temperature dependence of magnetic susceptibility was determined from room temperature up to 700°C for eight samples of different color with an automated CS-23 furnace attached to a KLY-2 magnetic susceptibility bridge (AGICO Ltd., Czech Republic). Heating and cooling curves were measured in air employing a heating rate of 11°C/min. Curie/Néel temperatures ( $T_C$ ,  $T_N$ ) of the dominant (anti)ferromagnetic minerals were determined from the minimum at the first derivative of the heating curve (Fabian et al., 2013; Petrovský & Kapička, 2006).

Magnetic mineralogy of differently colored daub materials was also characterized by stepwise acquisition of isothermal remanent magnetization (IRM) up to 5 Tesla field for 4 samples using an IM-10-30 pulse magnetizer (ASC Scientific, USA). Remanences were measured with a JR6A automatic spinner magnetometer (AGICO Ltd., Czech Republic) with a sensitivity  $2 \times 10^{-6}$  A/m. For another 8 samples, IRM acquisition curves were measured with a vibrating sample magnetometer (VSM) EV9 VSM (DSM Magnetics, ADE Corp.) up to a maximum field of 2 Tesla. The IRM acquisition curves could be approximated by a distribution of cumulative Gaussian functions (Kruiver et al., 2001; Robertson & France, 1994). In our study the IRM acquisition curves were analyzed using MAG UnMix software by Maxbauer et al. (2016) for estimation of coercivity

distribution of the major magnetic components. Each coercivity component is characterized by its intensity; the field at which half of its intensity is reached ( $B_{1/2}$ ) and the parameter DP which characterizes the width of the distribution (Kruiver et al., 2001).

Hysteresis loops were measured for seven samples selected according to their color using a VSM Micromag 3900 (Princeton Measurements Corporation, USA) with maximum applied field of 1 T and using a EV9 VSM instrument (DSM Magnetics, ADE Corp.) up to a maximum field of 2 Tesla for another 3 samples. After correcting for paramagnetic contribution using the field interval between 0.7 and 2 T, the following magnetic parameters were obtained: saturation magnetization ( $M_s$ ), saturation remanence ( $M_r$ ), and coercive force ( $B_c$ ). Back-field remanence demagnetization curves were also measured in order to obtain the coercivity of remanence ( $B_{cr}$ ).

### 3.3. Magnetic Susceptibility Method for Determination of the Ancient Firing Temperature Applied to Archeological Burnt Daub

Iron (oxy)hydroxide transformations induced during heating are related to formation of new Fe-containing minerals which have different magnetic properties as compared to the initial minerals. Thus, the magnetic susceptibility—a basic magnetic characteristic—shows a sharp change (an increase or decrease) upon crossing the threshold temperature (i.e., the ancient firing temperature). These are the basic assumptions for estimation of maximum firing temperature according to the method of Rasmussen et al. (2012) which includes (i) stepwise heating of archeological daub samples from 300°C to progressively higher temperature up to 1,100°C, (ii) cooling down to room temperature, and (iii) measurement of magnetic susceptibility at room temperature after each heating step. Susceptibility data expressed as the squared value of the first derivative of magnetic susceptibility ( $(d\chi/dT)^2$ ) are plotted as a function of the refiring temperature. Sudden discontinuity in the curve marks the point when the original maximum firing temperature is exceeded. Reported accuracy of the method applied to pottery is  $\pm 26^\circ\text{C}$  (Rasmussen et al., 2012). The method anticipates that materials which have been heated in antiquity have already reached thermodynamic stability and mineralogical changes no more occur upon heating below the maximum temperature reached. Magnetic susceptibility also depends on the domain state and will be mostly influenced by the creation of a new superparamagnetic fraction (Maher, 1988), but we checked this possibility by monitoring changes in  $\chi_{fd}\%$  during stepwise heating and ensured that changes do not exceed 2–3% below the inferred maximum firing temperature. As discussed by Rasmussen et al. (2012), the method fails only for materials which do not contain Fe-bearing minerals. This is, however, a very uncommon situation. In our experimental setup additional measurements of the sample's weight after each temperature step were also performed. The experiment encloses 35 heating steps in total. The magnetic susceptibility signal after each refiring temperature is expressed on a mass-specific basis. In this way, the magnetic susceptibility reflects the change in the mineralogy which is often accompanied by changes in the material's porosity during heating (Wagner et al., 1998). Determination of ancient firing temperature using magnetic susceptibility (Rasmussen et al., 2012) was applied to a collection of 148 samples collected from 25 houses at the settlement site. Samples were selected to represent different visual color and texture.

### 3.4. Nonmagnetic Measurements

Chemical elemental composition was obtained for 9 selected samples through X-ray fluorescence analysis (XRF) using an energy-dispersive XRF spectrometer Spectro-X-Lab 2000 at ETH-Soil Chemistry (Zurich, Switzerland). The samples were ball-milled to fine powder and pressed pellets were prepared using 4 g of burnt daub and 0.9-g amide wax according to the geochemical procedure adopted in the laboratory. Element concentration obtained was converted to oxide content.

Diffuse reflectance spectroscopy (Scheinost et al., 1998) was employed for color analysis of 10 burnt daub samples. The spectra were measured on a Varian Cary 1E spectrophotometer equipped with a  $\text{BaSO}_4$ -coated integrating sphere and using  $\text{BaSO}_4$  as the white standard. Diffuse reflectance spectra were recorded from 380 to 710 nm in 0.5-nm steps. The spectra obtained were used for calculation of tristimulus values (X, Y, Z), Value, and Chroma using free Munsell Conversion Software (<http://WallKill.Color.com>).

Qualitative bulk-sample X-ray powder diffraction (XRD) analysis of four burnt daub samples and one sediment sample were carried out with a Siemens D5000 XRD system with monochromatic  $\text{Co K}\alpha$

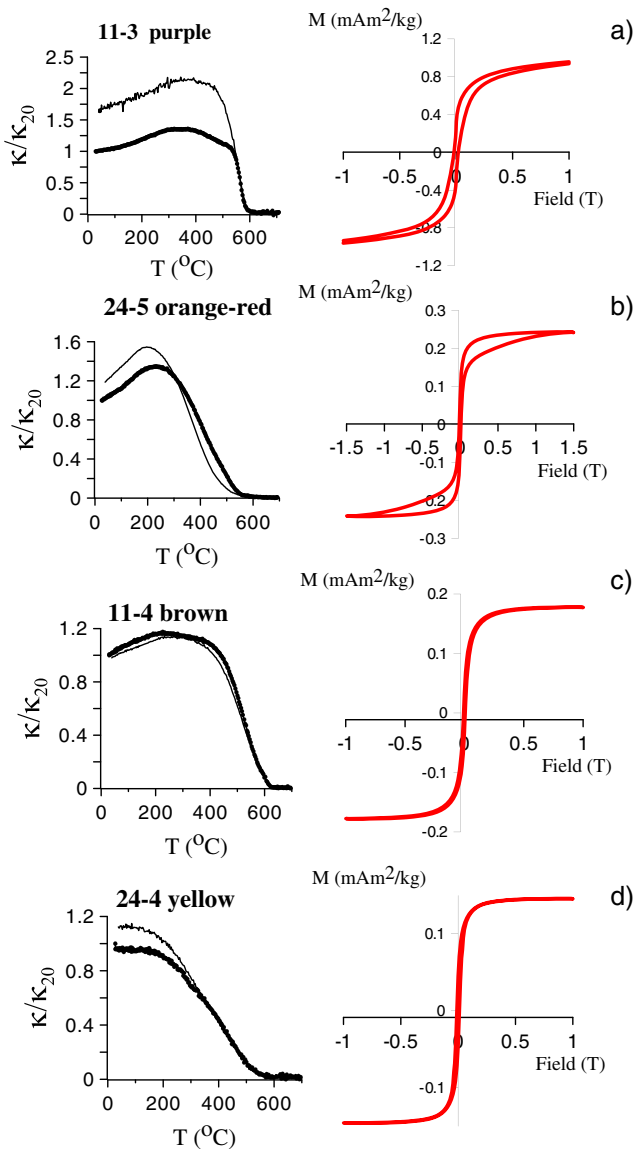


**Figure 2.** Representative examples of thermomagnetic analyses of magnetic susceptibility for samples of different color and hysteresis loops. Thick black curve—heating run, thin black curve—cooling run. Hysteresis curves after correction for paramagnetic contribution.

( $\lambda = 0.179$  nm; 40 kV, 25 mA) radiation. Polished sections were prepared from daub samples of purple and red-orange color for SEM observations. SEM observations coupled with energy-dispersive X-ray analysis (EDS) in selected spots were performed on a JEOL JSM6390 electron microscope in backscattered electrons mode. One raw sample from a vitrified daub piece was mounted on epoxy resin and also used for SEM observations.

## 4. Results

### 4.1. Magnetic Mineralogy of Burnt Daub Remains From Neolithic Houses

High-temperature behavior of magnetic susceptibility is particularly useful for the identification of trace amounts of iron oxide minerals in natural materials (Oldfield, 1999). A set of samples representing the most frequently observed types of burnt daub remains from Mursalevo-Deveboaz were analyzed using this technique. Representative examples for the major color classes of the daub material are shown in Figure 2. Normalized to the initial room temperature magnetic susceptibility value, heating-cooling curves indicate little mineralogical transformations upon heating up to 700°C and further cooling, as revealed by almost unchanged shape of the cooling run (Figures 2b–2d). An exception is sample 11-3 (Figure 2a), which comes from a vitrified purple-colored piece of daub. This thermal instability of the material could be linked to thermodynamic disequilibrium during ancient fire resulting from significantly different heating/cooling regimes in the past and in the laboratory conditions. As demonstrated by Jordanova and Jordanova (2016), reversibility of high-temperature magnetic susceptibility curves depends on the heating rate as well. Moreover, an experimental study simulating archeological fire (Brodard et al., 2015) evidenced that extremely high temperatures (over 900°C) are reached almost instantaneously and persist only for short time during burning. The main Curie temperatures ( $T_c$ ) vary between 520 and 570°C, suggestive of Ti-poor titanomagnetite as a main ferromagnetic mineral. The purple sample 11-3 (Figure 2a) shows quite a sharp decrease close to the  $T_c$ , thus indicating also a narrow grain-size distribution of the assemblage of the ferrimagnetic grains or the presence of large multidomain grains. For the orange-red and yellow samples (Figures 2b and 2d),  $\chi$  decrease starts already after  $\sim 350^\circ\text{C}$  and therefore indicates a wider grain size spectrum of these ferrimagnetic phases. Hysteresis curves are of ferrimagnetic type for brown and purple materials, while orange-red samples all exhibit wasp-waisted hysteresis loops (Figure 2b, right-handed graphs). A summary of the hysteresis parameters obtained as well as the percent frequency-dependent magnetic susceptibility ( $\chi_{fd}\%$ ) are shown in Table 1. Samples from purple-colored vitrified material show the highest  $M_s$  and  $M_{rs}$  values and two samples out of four measured have distorted loops (a wasp-waisted and a potbellied one). At the same time, they show relatively low  $\chi_{fd}\%$  values, varying between 1% and 4% (Table 1). The samples from this group exhibiting distorted hysteresis loops show the highest  $B_{cr}$  and  $B_c$  values. The yellow-colored sample 24-4 is weakly magnetic (relatively low  $M_{rs}$  and  $M_s$ ) and magnetically soft (Table 1), with low  $\chi_{fd}\%$ . Burnt daub material with orange-red coloring shows consistent hysteresis characteristics with  $B_c \sim 10$  mT and  $B_{cr} \sim 35$  mT, while  $\chi_{fd}\% \sim 12\%$ .

Representative IRM acquisition curves and coercivity components extracted are shown in Figure 3. In purple- and red-orange-colored samples, IRM clearly contains a high-coercivity fraction, in addition to a magnetically soft component (Figures 3a and 3b). On the other hand, brown- and yellow-colored samples almost reach

**Table 1**

*Hysteresis Parameters (Coercive Force [ $B_c$ ], Saturation Magnetization [ $M_s$ ], and Saturation Remanent Magnetization [ $M_{rs}$ ]), Coercivity of Remanence ( $B_{cr}$ ), Specification of the Hysteresis Loop's Shape, Percent Frequency-Dependent Magnetic Susceptibility ( $\chi_{fd}\%$ ), and Ratios  $B_{cr}/B_c$  and  $M_{rs}/M_s$  for Selected Samples*

Sample no	Color	$B_c$ (mT)	$B_{cr}$ (mT)	$M_s$ (mAm <sup>2</sup> /kg)	$M_{rs}$ (mAm <sup>2</sup> /kg)	Hysteresis loop shape	$\chi_{fd}\%$	$B_{cr}/B_c$	$M_{rs}/M_s$
11-3	Purple	19.1	68.2	940.80	281.40	WWL	4	3.57	0.30
11-10	Purple	7.8	16.6	819.48	185.52		3	2.14	0.23
11-11	Purple	17.1	33.9	893.26	258.99		1	1.98	0.29
24-3	Purple	19.8	55.9	679.57	68.02	Potbelly	2	2.83	0.10
11-15	Orange-red	11.5	39.3	173.45	49.27	WWL	12	3.42	0.28
24-5	Orange-red	10.5	32.8	241.63	67.22	WWL	12	3.11	0.28
17-12	Orange-red	10.9	34.8	433.10	93.14	WWL	11	3.20	0.22
11-4	Brown	6.7	18.9	177.48	32.71		6	2.84	0.18
24-4	Yellow	10.9	20.6	145.67	45.27		3	1.89	0.31
24-12	Yellow/light brown	6.8	43.4	226.80	29.20	WWL	10	6.37	0.13

Note. WWL, wasp-waisted shape of hysteresis curve.

saturation in fields as low as 100 mT (Figures 3b and 3d). Two components were identified in the samples of low and high coercivity, respectively. These two coercivity components are particularly well separated in the orange-red sample No. 11-15 (Figure 3b), while in the rest of the samples, the contribution of the high-coercivity component is weaker. The results from the coercivity component analysis for all 10 samples examined are shown in Table S1 in the supporting information. The coercivity of the soft component varies across differently colored samples: It is the lowest in yellow- and brown-dominated materials (22–9 mT), higher in orange-red colored samples (30–40 mT), and the highest in purple (vitrified) materials (36–64 mT). The coercivity of the magnetically harder component also varies, being the lowest in the brown samples (350–420 mT), and the highest (reaching 1,260 mT) in purple materials (Table S1). This systematic change in the coercivity parameters could be linked to differences in the samples' color and firing temperatures, as will be discussed later.

#### 4.2. Mineralogical and Elemental Composition of Raw Clay and Burnt Daub

Qualitative bulk powder XRD analysis of a sediment sample shows that the raw clay material contains quartz, feldspar, mica, kaolinite, and calcite, while burnt daub samples do not contain calcite. Several burnt samples with different dominating colors were subjected to an XRF analysis for determination of their bulk chemical composition. The results obtained for the major elements (Table 2) show that the most important difference in the chemical composition is the CaO content. It clearly discriminates the samples of different color; the highest CaO is obtained in yellow-colored samples, followed by brown- and purple-colored burnt daub, while CaO is the lowest in orange-red samples. Silica (SiO<sub>2</sub>) makes up between 43 and 59 wt% of the samples, but no systematic distinction among the differently colored samples is observed (Table 2). The total iron content expressed as Fe<sub>2</sub>O<sub>3</sub> varies between 4.7 and 6.2 wt % and also has no link with the sample's color.

#### 4.3. Scanning Electron Microscopy Observations and Point EDS Analyses

Scanning electron microscopy observations on a polished section of a purple-colored burnt daub sample (Figure 4a) and a nonpolished piece (Figure 4c) reveal the morphology typical of high-temperature vitrification processes: presence of large voids due to gaseous phase evaporation, melting, and formation of dendrite-like structures (Figure 4b). A higher-resolution zoom into a nonpolished sample (Figure 4d) shows high resemblance to the so-called "ceramic wood" or "porous ceramics" (Bantsis et al., 2012; Liu et al., 2007; Mizutani et al., 2005) employed nowadays for thermal insulation, high-temperature filtration, catalysis, etc. EDS analyses in selected spots denoted by numbers in Figure 4 give further insight into the chemical composition of the different parts of the sample (Tables S2 and S3). The material is very inhomogeneous, porous, and enriched mainly in SiO<sub>2</sub>, CaO, MgO, and FeO in its different parts (Tables S2 and S3). The orange-red colored sample (Figure 4e) displays sharp grain boundaries and morphologies without signs of vitrification. Typical exsolution structures enriched in FeO are observed, while the darker areas (in BSE mode) contain more Al<sub>2</sub>O<sub>3</sub> (Tables S2 and S3).

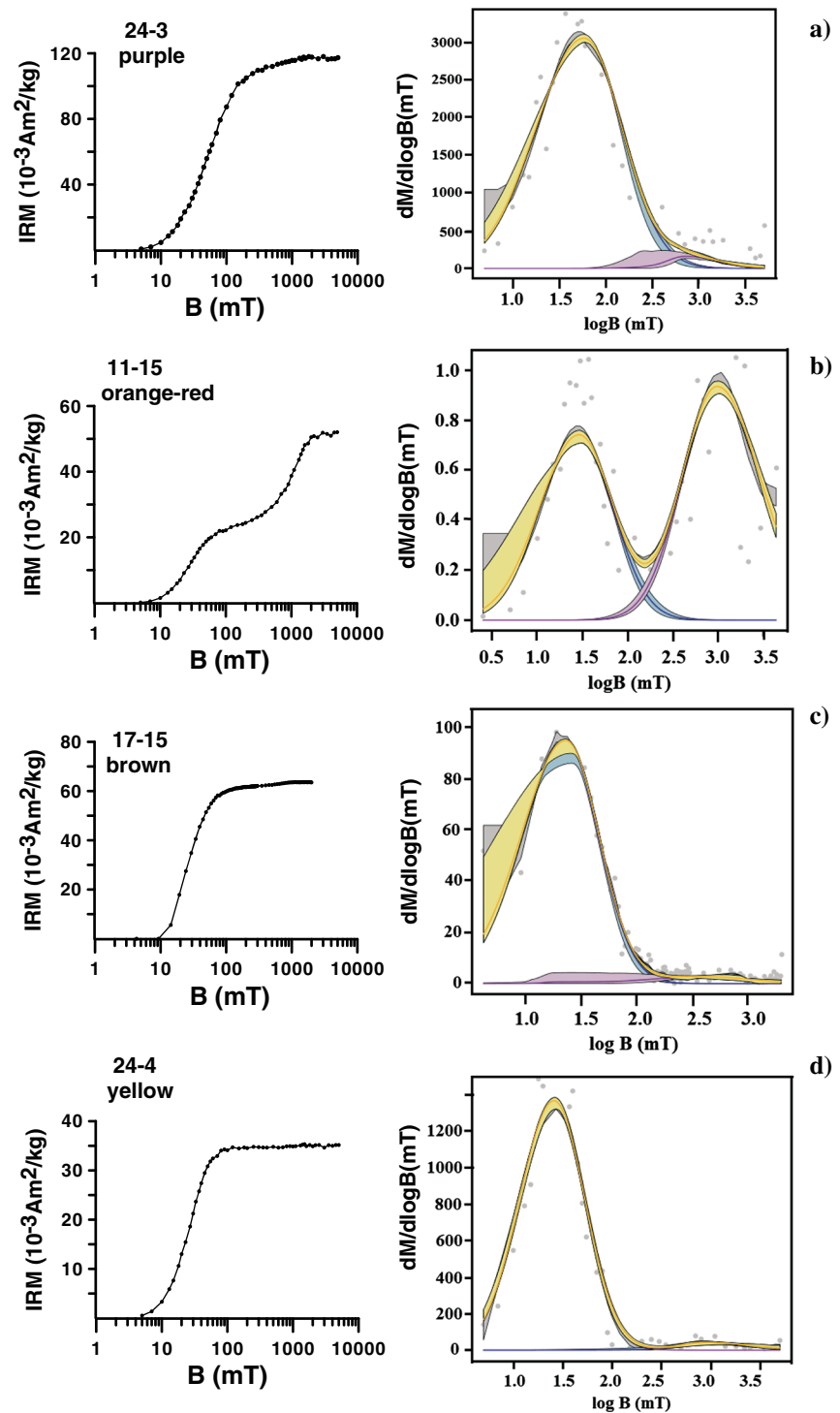


**Figure 3.** Examples of isothermal remanent magnetization acquisition up to 5-T field and the unmixed coercivity components using MAX UnMix software by Maxbauer et al. (2016). Data points are denoted by dots; cumulative fit together with its confidence band is shaded in yellow.

#### 4.4. Magnetic Susceptibility of Burnt Daub From Mursalevo-Deveboaz

Burnt daub materials from the site show a wide range of variations of mass-specific low-field magnetic susceptibility: from  $\chi \sim 30 \times 10^{-8} \text{ m}^3/\text{kg}$  to  $\chi \sim 2,000 \times 10^{-8} \text{ m}^3/\text{kg}$ . Histograms of the distribution of  $\chi$  and  $\chi_{rd}\%$  are shown in Figures 5a and 5b. Magnetic susceptibility shows a distribution close to normal, though the  $\chi^2$

**Table 2**  
Elemental Composition Determined on Bulk Samples Using X-ray Fluorescence Analysis

Sample	Color	Na <sub>2</sub> O	MgO	K <sub>2</sub> O	CaO	SiO <sub>2</sub>	Al <sub>2</sub> O <sub>3</sub>	TiO <sub>2</sub>	MnO	Fe <sub>2</sub> O <sub>3</sub>	P <sub>2</sub> O <sub>5</sub>	S (μg/g)
11-10	Purple	2.20	1.83	3.04	3.99	59.17	14.45	0.71	0.09	5.64	0.42	466.8
24-1	Purple	2.30	1.79	3.23	5.31	58.34	13.56	0.65	0.09	5.07	0.74	178.7
24-3	Purple	2.32	1.65	3.07	4.00	59.43	14.07	0.67	0.11	5.40	0.55	457.8
11-15	Orange-red	2.14	2.46	2.55	2.65	59.28	15.76	0.69	0.09	5.81	0.47	198.2
17-12	Orange-red	0.89	2.92	2.61	2.84	51.36	16.62	0.70	0.08	5.98	0.72	242.3
17-15	Brown	1.28	2.39	2.38	5.02	46.91	15.05	0.61	0.09	6.22	1.14	220.0
24-8	Brown	0.75	2.48	2.61	5.92	49.76	14.76	0.68	0.10	5.49	0.83	479.8
24-12	Yellow	2.11	2.31	1.89	12.93	51.68	13.62	0.58	0.08	4.83	0.41	452.1
24-4	Yellow	0.97	2.14	1.76	12.38	43.85	10.75	0.48	0.07	4.73	0.45	740.2

Note. Elements expressed as oxides in weight %.

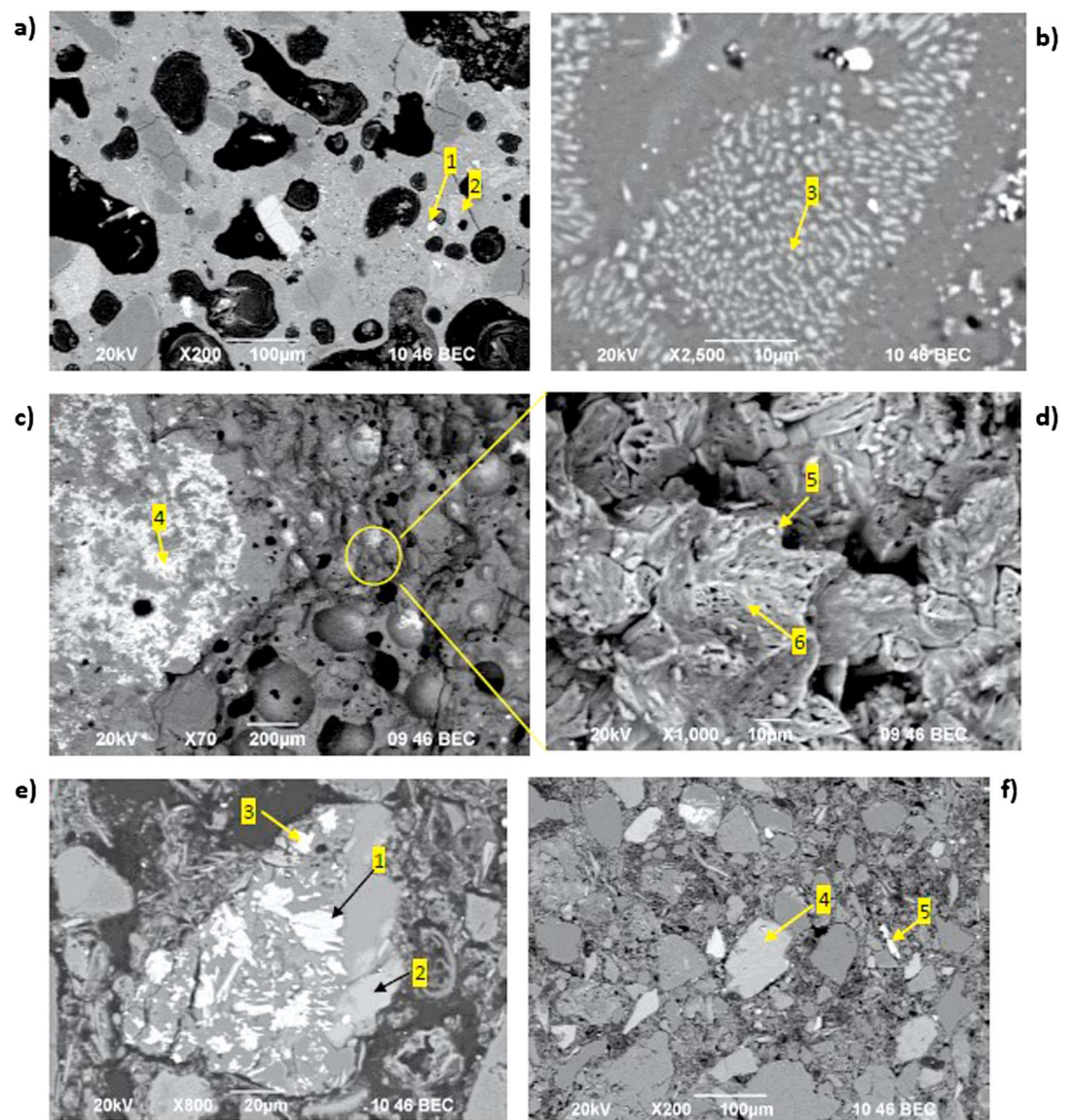


**Figure 4.** (a and b) Microphotographs of the polished sample of vitrified purple burnt daub material using scanning electron microscopy (SEM) in back scattered electrons mode. The numbers indicate spots for the energy-dispersive X-ray (EDS) analyses reported in Table S2. (c) The image is taken at the nonpolished sample; (d) the image is a magnified view of the encircled area in (c); (e and f) SEM image of orange-red burnt daub with spots for the EDS analyses (Table S3).

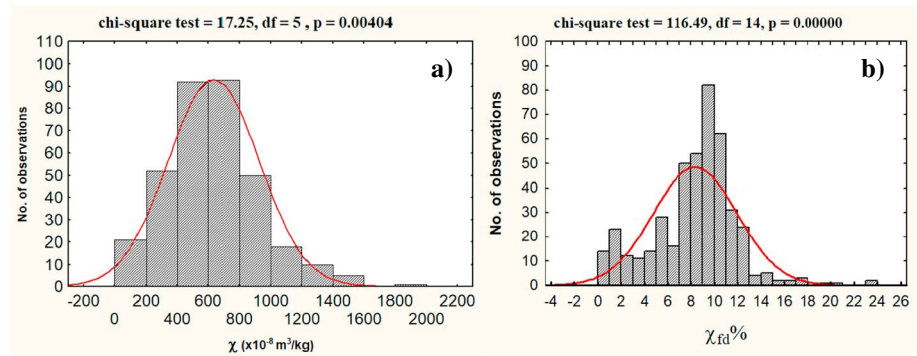


**Figure 5.** Distributions of measured values of (a) mass-specific magnetic susceptibility and (b) percent frequency dependent magnetic susceptibility ( $\chi_{fd}\%$ ) for the burnt daub samples. Total number of samples: 349. The red line represents the expected normal distribution of the values.

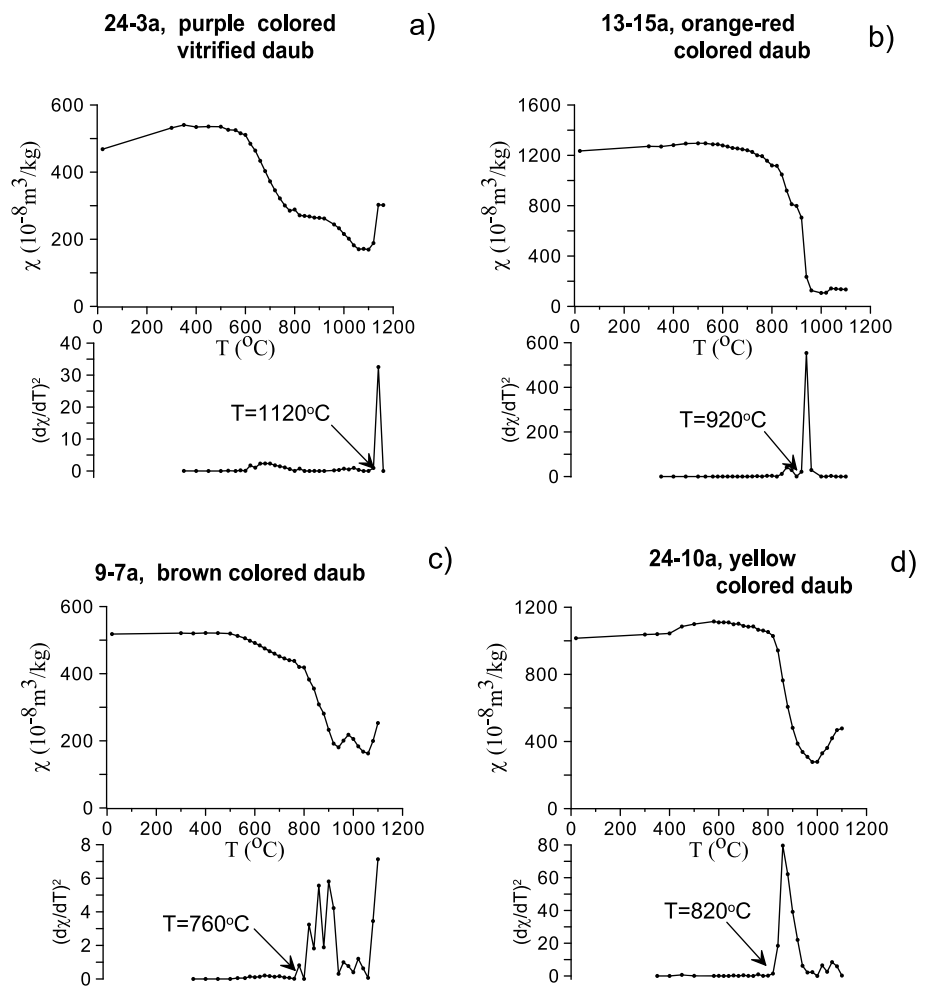


**Figure 6.** Examples for room temperature magnetic susceptibility values measured after each laboratory heating step from 300°C up to 1,180°C and the corresponding squared first derivative of the signal with determined maximum firing temperature for (a) purple colored daub sample, (b) orange-red colored burnt daub samples, (c) brown-colored burnt daub samples, and (d) yellow colored daub sample.

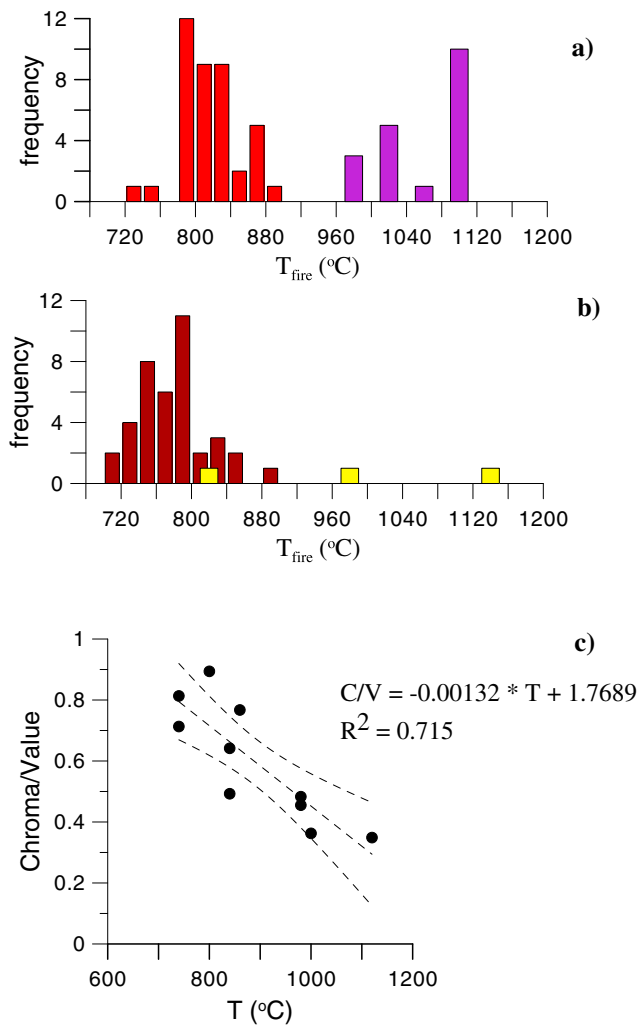


**Figure 7.** Ancient firing temperatures of burnt daub of different color: (a—orange-red and purple and b—brown and yellow) distribution of the obtained maximum firing temperatures separated according samples' color (number of samples per group: brown  $N = 45$ , orange-red  $N = 48$ , purple  $N = 19$ , and yellow  $N = 3$ ); (c) relationship between the estimated firing temperature and the Chroma/Value (C/V) ratio obtained from diffuse reflectance spectra for representative burnt daub samples. The regression equation with corresponding  $R^2$  estimate and the 95% confidence interval (dashed envelope of the linear regression line) are shown as well.

laps, but nonetheless, the maxima in their distributions are shifted, being higher for the orange-red colored materials. The purple-colored (vitrified) materials form a separate group with maximum firing temperatures above 1,000°C (Figure 7a).

#### 4.6. Magnetic Susceptibility Profile of Sediment Deposits

Magnetic susceptibility obtained for the sediment samples from different depths varies between  $30$  and  $80 \times 10^{-8} \text{ m}^3/\text{kg}$  as shown in Figure S4. During incremental laboratory heating of this material, supposed to represent the most probable raw clay for house construction, magnetic susceptibility increases after heating at a temperature of 800°C (Figure S4), but this increase does not reach the typical magnetic enhancement obtained for burnt daub (Figure 5a). Therefore, it may be hypothesized that raw clay was probably mixed with organic additives which provoked stronger magnetic enhancement of daub during burning.

test shows  $\chi^2 = 23.27$ , which is just above the critical value of  $\chi_{\text{crit}}^2 = 23.2$ . Two groups of samples could be distinguished—one with a relatively low  $\chi$  where most of the samples have  $\chi \sim 200\text{--}300 \times 10^{-8} \text{ m}^3/\text{kg}$ , and a second group with a maximum  $\chi$ -occurrence centered at about  $500\text{--}700 \times 10^{-8} \text{ m}^3/\text{kg}$  (Figure 5a). A tail extending toward extremely high  $\chi > 1,000 \times 10^{-8} \text{ m}^3/\text{kg}$  contains about 50 samples. Frequency-dependent magnetic susceptibility  $\chi_{\text{fd}}\%$  spans a wide range: from zero to  $\sim 20\%$ . Frequency distribution of  $\chi_{\text{fd}}\%$  shows three possible subgroups with maxima at  $\sim 2\%$ ,  $6\%$ , and  $10\%$  (Figure 5b). Twenty samples show a very high  $\chi_{\text{fd}}\%$  above  $12\%$  (Figure 5b). The lack of a normal distribution is evidenced also by the  $\chi^2$  test, revealing a  $\chi^2$  value of 116.49, which is much larger than the critical estimate of  $\chi_{\text{crit}}^2 = 32.8$ .

The spatial distribution of mass-specific magnetic susceptibility based on laboratory sample measurements is shown in Figure S4. It is seen that extremely high magnetic susceptibilities ( $\chi > 700 \times 10^{-8} \text{ m}^3/\text{kg}$ ) are found in all houses studied regardless of their age.

#### 4.5. Determination of Ancient Firing Temperatures With the Magnetic Susceptibility Method

Several representative examples from the experiment for ancient firing temperature determination from the major daub color classes (purple, orange-red, brown, and yellow) identified in the collection are shown in Figure 6, and a list of all determined firing temperatures is provided in Data Set S1. The lowest firing temperatures were obtained for the group of brown-colored burnt daub pieces (Figure 6c). The orange-red colored materials commonly exhibit high initial magnetic susceptibilities (Figure 6b) and a similar behavior during stepwise laboratory heating. Firing temperature estimates reach 920°C (Figure 6b). Magnetic susceptibility behavior of purple vitrified daub during stepwise heating shows two distinct features depending on the initial  $\chi$  value (Figure S3). Nevertheless, the estimated firing temperatures lie all around and above 1,000°C (Figures 6a and S3). The yellow-colored samples show the most diverse behavior of  $\chi$  during stepwise heating (Figure 6d), and the firing temperatures determined also vary.

Histograms representing the obtained ancient firing temperatures from burnt daub of different color are shown in Figures 7a and 7b. It is obvious that the frequency distribution is not unimodal and has two maxima: the biggest part of the examined samples showed firing temperatures in the interval 800–850°C (Figures 7a and 7b). The frequency distribution of brown- and orange-red colored burnt daub largely overlaps,

## 5. Discussion

### 5.1. Magnetic Minerals Identified in Burnt Daub and Their Origin

As revealed by the diagnostic magnetic experiments (Figures 2 and 3 and Table 1), the main iron oxide phases identified in the burnt daubs from Mursalevo-Deveboaz are magnetite/maghemite and hematite, found in a varying proportion in differently colored samples. A strongly magnetic phase dominating the magnetic susceptibility, magnetization (Figure 2), and isothermal remanence (Figure 3) may be linked either to the presence of magnetite with certain foreign-ion substitutions (Jiang et al., 2016) or to maghemite with aluminum substitutions (Dunlop & Özdemir, 1997; Özdemir & Banerjee, 1984) which is thermally stable against conversion to hematite. Considering the results from the thermomagnetic analysis and the hysteresis parameters (Figure 2 and Table 1), it could be supposed that the magnetically softer phase in the purple-colored burnt daub is most probably magnetite of stable single-domain (SD) to pseudo single domain state, taking into account the relatively narrow drop in  $\chi$  close to the  $T_c$ , in combination with high saturation magnetization ( $M_s$ ) values and the highest coercivities ( $B_c$  and  $B_{cr}$ ) as compared to the other samples (Table 1). This conclusion is supported also by the lowest  $\chi_{fd}\%$  obtained for purple-colored materials, since stable SD grains do not show frequency dependence of magnetic susceptibility (Worm, 1998). The high-coercivity phase in orange-red and purple-colored materials could be linked to the formation of ultrafine grains of hematite produced during firing, resembling the products of self-sustained combustion of iron-sulfate in the presence of organic fuel (Deshpande et al., 2004; Mariani et al., 2017; Opuchovic & Kareiva, 2015). According to the cited works, variously colored ultrafine hematite particles were obtained through calcinations at different temperatures of a mixture of iron salt (in this case, Fe-sulfate) and citric acid (or another organic acid). Purple-colored hematite had been formed on heating the mixture above 900–1,000°C, which is also accompanied by material bloating (Mariani et al., 2017). The color and properties of the vitrified purple-colored material found at many places in the burnt houses at Mursalevo-Deveboaz markedly resemble the bloated hematite pigments described in the cited works. The hematite phase, identified through our magnetic experiments, is most unambiguously revealed in the orange-red colored materials through its coercivity (Figure 3b). High remanence coercivity values of  $B_{1/2}$  (700–1,000 mT) suggest that hematite is of ~SD/pseudo single domain grain size which is compatible with its supposed firing-induced origin. Red-colored hematite of high coercivity has been also reported to form from carbonated ferrihydrite during heating at different calcinations temperatures (Vallina et al., 2014) producing single nanocrystals at lower temperatures (350–600°C) and larger aggregated particles (but still in the SD region) upon heating to 800–1,000°C. Brown-colored burnt daub contains a minor amount of hematite which is not detected on the thermomagnetic curves (Figure 2c). The coercivity of this hematite is considerably lower compared to that in the orange-red or purple-colored materials (Table S2), suggesting that it is probably of a grain size at the boundary between SD and SP states (Özdemir & Dunlop, 2014) where  $B_{cr}$  sharply decreases. Therefore, magnetic grain size data show an increasing size of both magnetite/maghemite and hematite particles formed during daub burning from SP toward SD magnetic grain size with increasing burning temperature. Yellow-colored materials usually show weak magnetization and magnetic susceptibility and are frequently observed around spots of vitrified purple-colored material (Figure 1b) and it might be supposed that it is linked to the process producing this high temperature feature. However, exactly the yellow-colored materials contain the highest amount of CaO (Table 2), in contrast to all the other samples. In order to explain this difference, we can use the findings reported in Gredmaier et al. (2011) showing that a black reduced core (enhanced in magnetite) in bricks is surrounded by a calcium sulfate layer formed during firing. Similarly, we suppose that the yellow-colored burnt material is enriched in calcium sulfate, which is supported by the fact that these samples also contain the highest amount of sulfur (Table 2). As Gredmaier et al. (2011) suggest, when  $\text{CaCO}_3$  is present in the clay during firing, Ca reacts with S after expulsion of  $\text{CO}_2$  at 800–900°C, thus forming Ca-sulfate.

### 5.2. Paleo-Firing Temperatures at the Neolithic Settlement

The ancient firing temperatures at the Neolithic site of Mursalevo-Deveboaz estimated using the magnetic susceptibility method (Rasmussen et al., 2012) provide ample proof of intense fires involving the majority of the houses, since the lowest firing temperatures exceed 700°C (Figures 7a and 7b). As is also evident from Figures 7a and 7b, the temperatures obtained are clearly linked to the burned daub's color, which in turn is mainly governed by the iron oxide phase (Murad & Wagner, 1998). This line of reasoning is also utilized for estimations of firing temperatures in burned prehistoric houses (Stevanović, 1997). On the other hand,

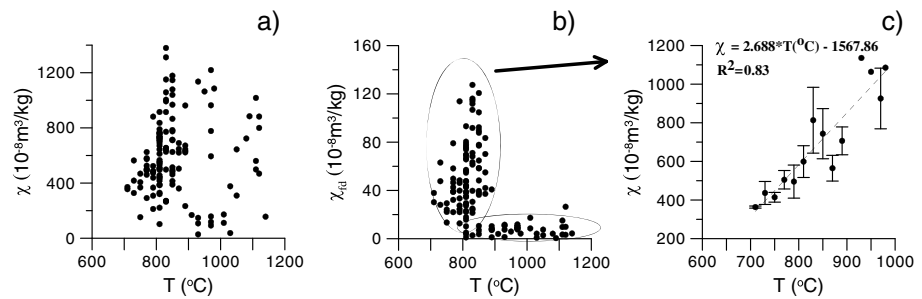


**Figure 8.** Scatterplots of determined firing temperatures against (a) initial mass-specific magnetic susceptibility of the burnt daubs, (b) frequency dependent magnetic susceptibility ( $\chi_{fd}$ ), and (c) mean  $\chi$  values with the corresponding standard deviation for samples showing  $\chi_{fd} > 10 \times 10^{-8} \text{ m}^3/\text{kg}$ . The dashed line represents the fitted linear regression to the data.

evaluations based on Munsell color chart determinations are subjective since any observer could assign slightly different color notation, leading to respective differences in the temperatures obtained. We have compared the estimated firing temperatures obtained by the magnetic susceptibility method and color parameters, calculated from diffuse reflectance spectra for 10 pilot samples, using the ratio Chroma/Value (Figure 7c). The obtained relatively well-defined linear regression ( $R^2 = 0.71$ ) suggests that indeed firing temperatures greatly affect the color of the burned daub. On the other hand, it is well known that the calcium content has significant influence on the color of the burned clay (Maniatis, Simopoulos, & Kostikas, 1981). Therefore, magnetic measurements could provide an alternative physical basis for correct estimation of the firing temperatures.

Based on the large analytical data set for the firing temperatures ( $T_{\text{fire}}$ ) across the settlement, the spatial distribution of  $T_{\text{fire}}$  provides further details related to fire intensity in the different houses. One of the major limiting factors for the application of the magnetic susceptibility method, however, is linked to the necessary choice how to balance between the desired accuracy in  $T_{\text{fire}}$  estimate and the time required for performing many-fold heating-cooling runs with successive susceptibility measurements in the laboratory. Thus, larger temperature increments will provide faster but not so precise estimate and vice versa. On the other hand, magnetic susceptibility measurement is very fast and easily attainable. We therefore looked for a potential link between the firing temperatures obtained and the magnetic susceptibility of the samples. Simply plotting the magnetic susceptibility values against the obtained firing temperatures (Figure 8a) does not reveal a systematic relation between the two parameters. However, frequency-dependent magnetic susceptibility ( $\chi_{fd}$ ) versus  $T_{\text{fire}}$  shows the presence of two groups of samples: one comprising the majority of samples with a big dispersal of  $\chi_{fd}$  and a second one characterized by  $\chi_{fd}$  as low as  $10 \times 10^{-8} \text{ m}^3/\text{kg}$  and generally very high  $T_{\text{fire}}$  (Figure 8b). For the first group of samples, we estimated the average value of  $\chi$  for samples showing certain  $T_{\text{fire}}$  using 20°C interval (e.g., 700, 720, 740°C, etc.). The result is plotted in Figure 8c along with the standard deviation in  $\chi$ . A good correspondence ( $R^2 = 0.83$ ) between the average magnetic susceptibility and the estimated  $T_{\text{fire}}$  is obvious. The biggest uncertainty and scatter in the data is seen for the susceptibility values of samples which have  $\chi_{fd}$  values close to the observed limit value of  $10 \times 10^{-8} \text{ m}^3/\text{kg}$  (Figure 8b). As a rule, all samples belonging to the second group with low  $\chi_{fd}$  values have purple, yellow, and, in rare cases, brown color. Thus, the results suggest that for samples having  $\chi_{fd} > 10 \times 10^{-8} \text{ m}^3/\text{kg}$ , there is a direct proportionality between the amount of strongly magnetic SP grains produced during fire (represented by  $\chi_{fd}$ ) and the maximum firing temperature achieved. Similar progressive increase in saturation magnetization ( $M_s$ ) and remanence ( $M_r$ ) during heating of calcium-rich clay above  $\sim 800^\circ\text{C}$  is reported by Beatrice et al. (2008), implying also an analogous increase in  $\chi$ . The relation obtained (Figure 8c) allowed us to construct a map of proxy-firing temperatures based on magnetic susceptibility measurements (Figure S6).

### 5.3. Archeological Implications of Paleo-Firing Temperatures Obtained in Mursalevo-Deveboaz Neolithic Settlement Site

Settlement sites characterized by the presence of abundant burnt houses are common in the later prehistory of Southeast Europe (Brami, 2014; Raczyk, 2014; Tringham, 2005). Burnt houses are found also in West Asia,

but in Anatolia and the Near East, they are constructed by sun-dried mud bricks (Akkermans et al., 2012; Forget et al., 2015; Forget & Shahack-Gross, 2016; Love, 2013), while in the Neolithic and Copper Age of Southeast Europe, the wattle-and-daub technique was most commonly used (Chapmann, 1999; Tringham, 2013). Wattle-and-daub construction of houses in antiquity is not restricted to southeastern Europe; it is found also in Neolithic sites in Pre-Hispanic Mesoamerica (Guerrero et al., 2016) and some areas of the pre-historic eastern and southeastern United States (Kruger, 2015). The houses uncovered at the Neolithic site of Mursalevo-Deveboaz were built mostly employing a wood-and-daub technique, and massive remains of sintered daub have been found (Figures 1b and S1 and S2). Extremely high firing temperatures in excess of 1,000°C are relatively frequently obtained (Figure 7a), as compared to the empirical study at the site of Opovo in Serbia (Stevanović, 1997). As Stevanović indicates, the highest firing temperatures are related to a two-story house. At Mursalevo-Deveboaz, almost all of the houses were two-story and thus the more frequent extreme temperatures obtained agree with Stevanović's conclusion.

In order to consider different factors which might have played a role in the burning of a Neolithic house, we have to take into account the fact that the raw clay for house construction was mixed with different additives (temper agents) which increase the clay plasticity and prevent cracking after drying (Kruger, 2015). The most common clay additive in ancient times as well as nowadays in many countries is animal dung, used also as fuel because of its high energy storage (Lancelotti & Madella, 2012; Shahack-Gross, 2011). Vitrified dung was found at some archeological sites in Africa (Huffman et al., 2013), and the authors conclude that dung deposits were most probably burned intentionally for hygienic and religious reasons. According to studies carried out by Peter (2001), vitrified dung occurrence is most probably related to the burning of a mixture of dung and urine. In the archeological literature, however, to the best of our knowledge, there is no analytical (chemical) consideration of the processes occurring during the burning of daub (clay mixed with dung and/or chaff), while a wealth of research is devoted to the elucidation of the chemical changes occurring in raw clay during firing (Cultrone et al., 2001; Maniatis et al., 1981; Wagner et al., 1998). On the other hand, much work has recently been focused on the synthesis of the nanosized iron oxides because of their multiple technological and medical applications (Deshpande et al., 2004; Gržeta et al., 2002). It has been proven that an efficient and cost-effective method for synthesis of nanosized materials is the solution combustion method (González-Cortés & Imbert, 2013; Mukasyan et al., 2007; Toniolo et al., 2007; Varma et al., 2016), which is also utilized in the preparation of Fe-based pigments (Mariani et al., 2017). The iron oxides produced are magnetite, maghemite, and hematite that have nanometer-sized grains and are characterized magnetically as superparamagnetic, growing to SD as the amount of fuel (and the temperature, respectively) increases (Toniolo et al., 2007; Varma et al., 2016). As it was evidenced by our rock-magnetic data, (Figures 2 and 3 and Table 1), the iron oxides detected in burnt daub materials from Mursalevo-Deveboaz are magnetite/maghemite and hematite of magnetic grain size increasing from SP to SD. Thus, a good correspondence between the magnetic characteristics with those of iron oxides obtained through solution combustion is at hand. In addition, color development from brown through orange-red toward purple fully agrees with the observations reported (Mariani et al., 2017; Opuchovic & Kareiva, 2015) for iron oxide pigments synthesized by solution combustion. In order to hypothesize the occurrence of solution combustion of this type during a Neolithic fire, we should consider the possibilities of producing the iron salts that can come into contact with fuel (i.e., organic acid) and water. Considering the daub composition as a mixture of soil (i.e., clay-rich substratum), dung, and urine (as discussed above), complex chemical species coexist there, involving urea,  $\text{NH}_4^+$ ,  $\text{NO}_3^-$  (van Groenigen et al., 2005), and Fe-ions liberated as a result of decreased pH (Cornell & Schwertmann, 2003). These are in fact the necessary compounds for a solution combustion reaction, involving ferrous sulfate (Mukasyan et al., 2007). Therefore, we suggest that a possible scenario which would explain the complex observations at Mursalevo-Deveboaz is an intentional house burning accomplished by additional supply of fuel in the form of dung and urine inside the building as well as outside of the house walls. Thus, the initiation of moderately intense fire at selected spots where fuel was piled would be enough to trigger and maintain the self-sustaining combustion incorporating also the wood-and-daub construction. Therefore, our hypothesis suggests that the obtained extremely high firing temperatures in the burnt houses at Mursalevo-Deveboaz were produced as a result of intentionally initiated burning leading to a self-sustaining combustion and production of fine nanometer-sized iron oxides with specific magnetic properties. Moreover, the observed specific texture of vitrified material closely resembling porous ceramics' features (Figure 4d) further supports the view that wood pillars in the houses were "impregnated" by solution

containing Fe ions. The above-mentioned porous ceramics are generally obtained through saturation of natural wood (the initial template) with Fe-containing solution, followed by calcinations at high temperature. As a result, the iron oxide ceramics develop sponge-like structures which mimic the morphology and the initial porous structure of the native wood (Bantsis et al., 2012; Liu et al., 2005). Integrating the above considerations about the mechanism of iron oxide production during the burning of the houses with the archeological evidence of deliberate and controlled house conflagrations, it seems reasonable to suggest that the Neolithic inhabitants of Mursalevo-Deveboaz possessed a very high degree of pyrotechnological knowledge.

## 6. Conclusions

An environmental magnetic study on burnt daub remains from the Neolithic settlement site of Mursalevo-Deveboaz (SW Bulgaria) provided independent analytical data about the firing conditions and probable mechanisms of iron oxide synthesis during ancient fire. Rock magnetic data on burnt daub from different houses show the presence of a large quantity of strongly magnetic iron oxides (magnetite/maghemite) as well as hematite, all of very fine (nanometer) grain size. Analytical estimations carried out with a rock magnetic approach demonstrate that the firing temperatures in the conflagrations at Mursalevo-Deveboaz vary between 680 and 1,140°C (depending on the color), thus reaching quite high values which suggests the occurrence of extremely intense fire in most of the houses. Based on simple magnetic measurements, detailed information about the degree of burning in the different structures was obtained. Comparison between the magnetic properties of burnt daub from Mursalevo-Deveboaz with experiments in material research related to solution-combustion synthesis of iron oxides, production of pigments, and porous iron oxides allowed us to hypothesize the mechanism behind the extreme firing observed at the Neolithic houses. We suggest that the Neolithic inhabitants of the site were aware of the conditions that guaranteed the most effective daub burning, and added dung and urine as supplementary fuel which provided all necessary compounds and conditions for combustion of the house construction and the extreme degree of daub burning observed during the archeological excavations. The occurrence of extremely high firing temperatures (in excess of 1,000°C) in different spots around most of the houses, combined with the archeological evidence, supports the theory of the deliberate house burning.

## Acknowledgments

This work was supported by the Bulgarian National Science Fund under Project DFNI K02/13. Additional data provided in the supporting information and Data Set S1. We are grateful to the Associate Editor Prof. Mark Dekkers and the two reviewers—E. Petrovský and A. Carrancho—for detailed and constructive comments which helped to improve the manuscript.

## References

- Akkermans, P., Brüning, M., Hammers, N., Huigens, H., Kruijer, L., Meens, A., et al. (2012). Burning down the house: The burnt building V6 at Late Neolithic Tell Sabi Abyad, Syria. *Analecta Praehistorica Leidensia*, 43(44), 307–324.
- Bantsis, G., Betsiou, M., Bourliva, A., Yioultsis, T., & Sikalidis, C. (2012). Synthesis of porous iron oxide ceramics using Greek wooden templates and mill scale waste for EMI applications. *Ceramics International*, 38(1), 721–729. <https://doi.org/10.1016/j.ceramint.2011.07.064>
- Barbetti, M. (1986). Traces of Fire in the Archaeological Record, Before One Million Years Ago? *Journal of Human Evolution*, 15, 771–781.
- Beatrice, C., Coisson, M., Ferrara, E., & Olivetti, E. S. (2008). Relevance of magnetic properties for the characterisation of burnt clays and archaeological tiles. *Physics and Chemistry of the Earth*, 33(6–7), 458–464. <https://doi.org/10.1016/j.pce.2008.02.018>
- Brami, M. (2014). House-related practices as markers of the Neolithic expansion from Anatolia to the Balkans. *Bulgarian e-Journal of Archaeology*, 4, 161–177.
- Brodard, A., Lacanette-Puyo, D., Guibert, P., Lévêque, F., Burens, A., & Carozza, L. (2015). A new process of reconstructing archaeological fires from their impact on sediment: A coupled experimental and numerical approach based on the case study of hearths from the cave of Les Fraux (Dordogne, France). *Archaeological and Anthropological Sciences*, 8(4), 673–687. <https://doi.org/10.1007/s12520-015-0250-7>
- Carrancho, Á., Herrejón-Lagunilla, Á., & Verges, J. M. (2016). Three archaeomagnetic applications of archaeological interest to the study of burnt anthropogenic cave sediments. *Quaternary International*, 414, 244–257. <https://doi.org/10.1016/j.quaint.2015.10.010>
- Chapmann, J. (1999). Deliberate house-burning in the prehistory of central and eastern Europe. In A. Gustafsson & H. G. Karlsson (Eds.), *Glyfer och arkeologiska rum: En vänbok till Jarl Nordbladh* (pp. 113–116). Durham, UK: University of Göteborg Press.
- Cornell, R., & Schwertmann, U. (2003). *The iron oxides. Structure, properties, reactions, occurrence and uses*. Darmstadt: Weinheim Wiley-VCH.
- Cultrone, G., Rodríguez-Navarro, C., Sebastian, E., Cazalla, O., & De La Torre, M. J. (2001). Carbonate and silicate phase reactions during ceramic firing. *European Journal of Mineralogy*, 13(3), 621–634. <https://doi.org/10.1127/0935-1221/2001/0013-0621>
- Deshpande, K., Mukasyan, A., & Varma, A. (2004). Direct synthesis of iron oxide nanopowders by the combustion approach: Reaction mechanism and properties. *Chemistry of Materials*, 16(24), 4896–4904. <https://doi.org/10.1021/cm040061m>
- Dunlop, D., & Özdemir, O. (1997). *Rock magnetism. Fundamentals and frontiers, Cambridge studies in magnetism*. Cambridge, UK: Cambridge University Press.
- Fabian, K., Shcherbakov, V. P., & McEnroe, S. A. (2013). Measuring the Curie temperature. *Geochemistry, Geophysics, Geosystems*, 14, 947–961. <https://doi.org/10.1029/2012GC004440>
- Forget, M., Regev, L., Friesemc, D., & Shahack-Gross, R. (2015). Physical and mineralogical properties of experimentally heated chaff-tempered mud bricks: Implications for reconstruction of environmental factors influencing the appearance of mud bricks in archaeological conflagration events. *Journal of Archaeological Science: Reports*, 2, 80–93. <https://doi.org/10.1016/j.jasrep.2015.01.008>
- Forget, M., & Shahack-Gross, R. (2016). How long does it take to burn down an ancient near eastern city? The study of experimentally heated mud-bricks. *Antiquity*, 90(353), 1213–1225. <https://doi.org/10.15184/aqy.2016.136>

- Gheorghiu, D. (2009). Built to be burnt: The building and combustion of Chalcolithic dwellings in the lower Danube and the Eastern Carpathian areas. In L. Nikolova, M. Merlini, & A. Comşa (Eds.), *Circumpontica in prehistory: Western Eurasian studies, BAR International Series* (pp. 55–68). Oxford: Archaeopress.
- González-Cortés, S., & Imbert, F. (2013). Fundamentals, properties and applications of solid catalysts prepared by solution combustion synthesis (SCS). Review. *Applied Catalysis A: General*, *452*, 117–131. <https://doi.org/10.1016/j.apcata.2012.11.024>
- Gredmaier, L., Banks, C. J., & Pearce, R. B. (2011). Calcium and sulphur distribution in fired clay brick in the presence of a black reduction core using micro X-ray fluorescence mapping. *Construction and Building Materials*, *25*(12), 4477–4486. <https://doi.org/10.1016/j.conbuildmat.2011.03.054>
- Grzeta, B., Ristić, M., Nowik, I., & Music, S. (2002). Formation of nanocrystalline magnetite by thermal decomposition of iron chlorine citrate. *Journal of Alloys and Compounds*, *334*(1–2), 304–312. [https://doi.org/10.1016/S0925-8388\(01\)01792-3](https://doi.org/10.1016/S0925-8388(01)01792-3)
- Guerrero, A. T., Goguitchaichvili, A., López, R. E., Morales, J., Elguera, J. R., Soler, A. M., et al. (2016). A detailed rock-magnetic and archaeomagnetic investigation on wattle and daub building (Bajareque) remains from Teuchitlán tradition (nw Mesoamerica). *Journal of Archaeological Science: Reports*, *5*, 564–573. <https://doi.org/10.1016/j.jasrep.2016.01.010>
- Harrison, K. (2013). The application of forensic fire investigation techniques in the archaeological record. *Journal of Archaeological Science*, *40*(2), 955–959. <https://doi.org/10.1016/j.jas.2012.08.030>
- Huffman, T. N., Elburg, M., & Watkeys, M. (2013). Vitriified cattle dung in the Iron Age of southern Africa. *Journal of Archaeological Science*, *40*(10), 3553–3560. <https://doi.org/10.1016/j.jas.2013.03.026>
- Jiang, Z., Liu, Q., Zhao, X., Roberts, A., Heslop, D., Barrón, V., & Torrent, J. (2016). Magnetism of Al-substituted magnetite reduced from Al-hematite. *Journal of Geophysical Research: Solid Earth*, *121*, 4195–4210. <https://doi.org/10.1002/2016JB012863>
- Jordanova, D., & Jordanova, N. (2016). Thermomagnetic behavior of magnetic susceptibility—Heating rate and sample size effects. *Frontiers in Earth Science*, *3*, 90. <https://doi.org/10.3389/feart.2015.00090>
- Kapper, K. L., Anesin, D., Donadini, F., Angelucci, D. E., Cavulli, F., Pedrotti, A., & Hirt, A. M. (2014). Linking site formation processes to magnetic properties. Rock- and archeomagnetic analysis of the combustion levels at Riparo Gaban (Italy). *Journal of Archaeological Science*, *41*, 836–855. <https://doi.org/10.1016/j.jas.2013.10.015>
- Kruger, R. A. (2015). Burning question or, some half-baked ideas: Patterns of sintered daub creation and dispersal in a modern wattle and daub structure and their implications for archaeological interpretation. *Journal of Archaeological Method and Theory*, *22*(3), 883–912. <https://doi.org/10.1007/s10816-014-9210-2>
- Kruiver, P., Dekkers, M., & Heslop, D. (2001). Quantification of magnetic coercivity components by the analysis of acquisition curves of isothermal remanent magnetization. *Earth and Planetary Science Letters*, *189*(3–4), 269–276. [https://doi.org/10.1016/S0012-821X\(01\)00367-3](https://doi.org/10.1016/S0012-821X(01)00367-3)
- Lancelotti, C., & Madella, M. (2012). The ‘invisible’ product: Developing markers for identifying dung in archaeological contexts. *Journal of Archaeological Science*, *39*(4), 953–963. <https://doi.org/10.1016/j.jas.2011.11.007>
- Liu, Z., Fan, T., Gu, J., Zhang, D., Gong, X., Guo, Q., & Xu, J. (2007). Preparation of porous Fe from biomorphic Fe<sub>2</sub>O<sub>3</sub> precursors with wood templates. *Materials Transactions*, *48*(4), 878–881. <https://doi.org/10.2320/matertrans.48.878>
- Liu, Z., Fan, T., Zhang, W., & Zhang, D. (2005). The synthesis of hierarchical porous iron oxide with wood templates. *Microporous and Mesoporous Materials*, *85*(1–2), 82–88. <https://doi.org/10.1016/j.micromeso.2005.06.021>
- Love, S. (2013). Architecture as material culture: Building form and materiality in the pre-pottery Neolithic of Anatolia and Levant. *Journal of Anthropological Archaeology*, *32*(4), 746–758. <https://doi.org/10.1016/j.jaa.2013.05.002>
- Maher, B. (1988). Magnetic properties of some synthetic sub-micron magnetites. *Geophysical Journal of the Royal Astronomical Society*, *94*, 83–96.
- Maniatis, Y. (2009). The emergence of ceramic technology and its evolution as revealed with the use of scientific techniques. In A. J. Shortland, I. C. Freestone, & T. Rehren (Eds.), *From mine to microscope: Advances in the study of ancient technology* (pp. 1–18). Oxford, UK: Oxbow Books.
- Maniatis, Y., Simopoulos, A., & Kostikas, A. (1981). Moessbauer study of the effect of calcium content on iron oxide transformations in fired clays. *Journal of the American Ceramic Society*, *64*(5), 263–269. <https://doi.org/10.1111/j.1151-2916.1981.tb09599.x>
- Mare, L. P., De Kock, M. O., Cairncross, B., & Mouri, H. (2016). Magnetic evaluation of the palaeothermal variation across the Karoo Basin, South Africa. *South African Journal of Geology*, *119*(2), 435–452. <https://doi.org/10.2113/gssajg.119.2.435>
- Mariani, F. Q., Borth, K. W., Müller, M., Dalpasquale, M., & Anaissi, J. F. (2017). Sustainable innovative method to synthesize different shades of iron oxide pigments. *Dyes and Pigments*, *137*, 403–409. <https://doi.org/10.1016/j.dyepig.2016.10.024>
- Maxbauer, D., Feinberg, J., & Fox, D. (2016). MAX UnMix: A Web application for unmixing magnetic coercivity distributions. *Computers & Geosciences*, *95*, 140–145. <https://doi.org/10.1016/j.cageo.2016.07.009>
- Mikov, V. (1932–1933). Materiali ot predistoricheskata epoha v Balgaria. *Izvestiya na Arheologicheskaya institute*, *7*, 362–363.
- Mizutani, M., Takase, H., Adachi, N., Ota, T., Daimon, K., & Hikichi, Y. (2005). Porous ceramics prepared by mimicking silicified wood. *Science and Technology of Advanced Materials*, *6*(1), 76–83. <https://doi.org/10.1016/j.stam.2004.08.004>
- Mukasyan, A., Epstein, P., & Dinka, P. (2007). Solution combustion synthesis of nanomaterials. *Proceedings of the Combustion Institute*, *31*(2), 1789–1795. <https://doi.org/10.1016/j.proci.2006.07.052>
- Murad, E., & Wagner, U. (1998). Clays and clay minerals: The firing process. *Hyperfine Interactions*, *117*(1/4), 337–356. <https://doi.org/10.1023/A:1012683008035>
- Nikolov, V., Bacvarov, K., Katsarov, G., Samichkova, G., Elenski, N., & Nikolova, N. (2016). Spasitelno arheologicheskoprochuvane na neolitnoto selishte v m. Deve boaz pri Mursalevo, obsht. Kocherinovo (AM “Struma,” LOT 2, obekt 15, ot km 346+300 do km 346+455). *Arheologicheski otkritia i razkopki prez 2015 g.* 72–75.
- Nikolov, V., Bacvarov, K., Takorova, D., Petrova, V., Samichkova, G., & Katsarov, G. (2015a). Spasitelno arheologicheskoprochuvane na neolitnoto selishte v m. Deve boaz pri Mursalevo, obsht. Kocherinovo (AM “Struma,” LOT 2, obekt 15) (ot km 346+300 do km 346+455). *Arheologicheski otkritia i razkopki prez 2014 g.* 45–47.
- Nikolov, V., Bacvarov, K., Takorova, D., Petrova, V., Samichkova, G., & Katsarov, G. (2015b). Spasitelno arheologicheskoprochuvane na ploshtta na stroitelnitate deynosti za kanalizatsionna sistema na Mursalevo v obhvata na iztochnata chast na neolitnoto selishte v m. Deve boaz. *Arheologicheski otkritia i razkopki prez 2014 g.* 48–50.
- Oldfield, F. (1999). The rock magnetic identification of magnetic mineral and grain size assemblages. In J. Walden, F. Oldfield, & J. Smith (Eds.), *Environmental magnetism: A practical guide Technical Guide No 6, Quaternary Research Association* (pp. 98–112). London.
- Opuhovich, O., & Kareiva, A. (2015). Historical hematite pigment: Synthesis by an aqueous sol-gel method, characterization and application for the colouration of ceramic glazes. *Ceramics International*, *41*(3), 4504–4513. <https://doi.org/10.1016/j.ceramint.2014.11.145>
- Özdemir, Ö., & Banerjee, S. (1984). High temperature stability of maghemite ( $\gamma$ -Fe<sub>2</sub>O<sub>3</sub>). *Geophysical Research Letters*, *11*(3), 161–164. <https://doi.org/10.1029/GL011i003p00161>

- Özdemir, Ö., & Dunlop, D. (2014). Hysteresis and coercivity of hematite. *Journal of Geophysical Research: Solid Earth*, *119*, 2582–2594. <https://doi.org/10.1002/2013JB010739>
- Peter, B. (2001). Vitriified dung in archaeological contexts: An experimental study on the process of its formation in the Mosu and Bobirwa areas, Pula. Botswana. *Journal of African Studies*, *15*, 125–143.
- Petrovský, E., & Kapička, A. (2006). On determination of the Curie point from thermomagnetic curves. *Journal of Geophysical Research*, *111*, B12S27. <https://doi.org/10.1029/2006JB004507>
- Raczky, P. (2014). Settlement in south-east Europe. In C. Fowler, J. Harding, & D. Hofmann (Eds.), *The Oxford handbook of Neolithic Europe* (pp. 235–253). New York: Oxford University Press. <https://doi.org/10.1093/oxfordhb/9780199545841.013.072>
- Rasmussen, K. L., De La Fuente, G., Bond, A., Mathiesen, K., & Vera, S. (2012). Pottery firing temperatures: A new method for determining the firing temperature of ceramics and burnt clay. *Journal of Archaeological Science*, *39*(6), 1705–1716. <https://doi.org/10.1016/j.jas.2012.01.008>
- Robertson, D. J., & France, D. E. (1994). Discrimination of remanence-carrying minerals in mixtures, using isothermal remanent magnetisation acquisition curves. *Physics of the Earth and Planetary Interiors*, *84*, 223–234.
- Salisbury, R. D., Bertók, G., & Bácsmegi, G. (2013). Integrated prospection methods to define small-site settlement structure: a case study from Neolithic Hungary. *Archaeological Prospection*, *20*, 1–10.
- Scheinost, A., Chavernas, A., Barron, V., & Torrent, J. (1998). Use and limitations of second-derivative diffuse reflectance spectroscopy in the visible to near-infrared range to identify and quantify Fe oxide minerals in soils. *Clays and Clay Minerals*, *46*(5), 528–536. <https://doi.org/10.1346/CCMN.1998.0460506>
- Shaffer, G. D. (1993). An archaeomagnetic study of a wattle and daub building collapse. *Journal of Field Archaeology*, *20*, 29–75.
- Shahack-Gross, R. (2011). Herbivorous livestock dung: Formation, taphonomy, methods for identification, and archaeological significance. *Journal of Archaeological Science*, *38*(2), 205–218. <https://doi.org/10.1016/j.jas.2010.09.019>
- Silva, P. F., Henry, B., Marques, F. O., Mateus, A., Madureira, P., Lourenço, N., & Miranda, J. M. (2006). Variation of magnetic properties in sedimentary rocks hosting the Foum Zguid dyke (southern Morocco): Combined effects of re-crystallization and Fe-metasomatism. *Earth and Planetary Science Letters*, *241*(3–4), 978–992. <https://doi.org/10.1016/j.epsl.2005.10.009>
- Stevanović, M. (1997). The age of clay? The social dynamics of house destruction. *Journal of Anthropological Archaeology*, *16*(4), 334–395. <https://doi.org/10.1006/jaar.1997.0310>
- Toniolo, J., Takimi, A., Andrade, M., Bonadiman, R., & Bergmann, C. (2007). Synthesis by the solution combustion process and magnetic properties of iron oxide (Fe<sub>3</sub>O<sub>4</sub> and  $\alpha$ -Fe<sub>2</sub>O<sub>3</sub>) particles. *Journal of Materials Science*, *42*(13), 4785–4791. <https://doi.org/10.1007/s10853-006-0763-7>
- Tringham, R. (2005). Weaving house life and death into places: a blueprint for a hypermedia narrative. In D. W. Bailey, A. Whittle, & V. Cummings (Eds.), *(Un)settling the Neolithic* (pp. 98–111). Oxford, UK: Oxford Oxbow.
- Tringham, R. (2013). Destruction of places by fire: Domicide or domithanasia. In J. L. Driessen (Ed.), *Destruction: Archaeological, philological, and historical perspectives* (pp. 89–108). Louvain, Belgium: Presses Universitaires de Louvain.
- Vallina, B., Rodriguez-Blanco, J. D., Brown, A. P., Benning, L. G., & Blanco, J. A. (2014). Enhanced magnetic coercivity of  $\alpha$ -Fe<sub>2</sub>O<sub>3</sub> obtained from carbonated 2-line ferrihydrite. *Journal of Nanoparticle Research*, *16*(3), 2322. <https://doi.org/10.1007/s11051-014-2322-5>
- van Groenigen, J. W., Kuikman, P. J., de Groot, W. J. M., & Velthof, G. L. (2005). Nitrous oxide emission from urine-treated soil as influenced by urine composition and soil physical conditions. *Soil Biology & Biochemistry*, *37*(3), 463–473. <https://doi.org/10.1016/j.soilbio.2004.08.009>
- Varma, A., Mukasyan, A. S., Rogachev, A. S., & Manukyan, K. V. (2016). Solution combustion synthesis of nanoscale materials. *Chemical Reviews*, *116*(23), 14,493–14,586. <https://doi.org/10.1021/acs.chemrev.6b00279>
- Verhoeven, M. (2000). Death, fire and abandonment. Ritual practice at late Neolithic Tell Sabi Abyad, Syria. *Archaeological dialogues*, *71*, 46–83.
- Wagner, U., Gebhard, R., Grosse, G., Hutzelmann, T., Murad, E., Riederer, J., et al. (1998). Clay: An important raw material for prehistoric man. *Hyperfine Interactions*, *117*(1–4), 323–335.
- Worm, H.-U. (1998). On the superparamagnetic—Stable single domain transition for magnetite, and frequency dependence of susceptibility. *Geophysical Journal International*, *133*(1), 201–206. <https://doi.org/10.1046/j.1365-246X.1998.1331468.x>
- Yang, T., Dekkers, M. J., & Zhang, B. (2016). Seismic heating signatures in the Japan Trench subduction plate-boundary fault zone: Evidence from a preliminary rock magnetic ‘geothermometer’. *Geophysical Journal International*, *205*, 332–344.